Journal of Computational Applied Mechanics 2023, 54(3): 378-389

DOI: 10.22059/JCAMECH.2023.363631.860

RESEARCH PAPER

Influence of spherical and cubical geometry of silver nanoparticles on thermal characteristics

Alireza Azizi [a], Anqiang Pan [a], Roya Momen [b,*]

[a] *School of Materials Science and Engineering, Central South University, Changsha, Hunan 410083, China*
[b] *Department of Chemistry and Shenzhen Grubbs Institute, Southern University of Science and Technology, Shenzhen 518055, China*

Abstract

Antibacterial activity of silver nanoparticles with spherical or cubic shapes in medical science will render it attractive. Considering the physical characteristics like thermal features as crucial factors are essential for choosing nanospheres or nanocubes with respect to operating temperature and stability. Therefore, this research probes the melting process, the surface premelting points (T_{sm}), the complete melting point (T_m), the phase transition, and the specific heat capacity at a constant volume (C_v) of silver nanospheres and nanocubes via a molecular dynamics approach. Regarding these aims, different approaches have been employed to achieve high accuracy. The results indicate that the geometry of nanoparticles dramatically influences the T_{sm} and T_m, and nanocubes have lower T_{sm} and T_m than nanospheres. Moreover, the nanocubes are melted from corners toward the cube center while the nanospheres melt in the radius direction. In contrast, C_v of silver nanospheres and nanocubes is almost identical, demonstrating that the C_v is independent of geometry. In addition, the values of C_v for the nanoparticles are close to the bulk value, which indicates that by changing the dimension of silver from bulk to nanoparticles, the specific heat capacity will not change, and this value is an intensive property.

Keywords: Melting process; Nanospheres; Nanocubes; Silver; Surface premelting; Specific heat capacity.

1. Introduction

The low-dimensional silver structures are mainly classified into three groups: nanoparticles (zero-dimensional) [1, 2], nanowires (one-dimensional) [3, 4], and nanofilms (two-dimensional) [5, 6]. These nanostructures, due to antimicrobial features [7], excellent optical [8] and electrical [9] characteristics, are utilized in the medical field [10], colorimetric sensors [11], and electronic devices [12]. In all of these applications, the morphology of the structure affected physical and chemical properties, specifically in the medical field. Hong et al. investigated the effect of silver nanostructures shape on the antibacterial activity [13]. They found out that the antibacterial activity is in the order of nanocubes > nanospheres > nanowires. Also, they expressed that these phenomena are observed because of effective

* Corresponding author. E-mail address: rmomen@sustech.edu.cn

contact areas between silver and bacteria. Since the order of the contact surface area and antibacterial activity is similar. This study indicates that for antibacterial applications, the use of nanoparticles (nanospheres and nanocubes) is worthy than nanowires. Silver nanospheres (AgNSPs) and nanocubes (AgNCs), owing to diverse morphology, the surface-to-volume ratio, and reactive facets exhibit different antibacterial and catalytic activities, thermal features, optical and electrical characteristics. Among these attributes, thermal properties are key factors that determine the operating temperature and thermal stability of nanoparticles [13-16]. Consequently, the previous researches investigated the thermal properties of silver nanoparticles with experimental and theoretical methods. Asoro et al. [17, 18], in experimental studies, probed the size effects of AgNSPs on melting temperature. They considered the diameter of AgNSPs between 5-50 nm and observed the melting point in the range of 723-993 K. It is evident that the melting point of AgNSPs is below the melting point of the silver bulk (1234 K) owing to their high surface-to-volume ratio and surface energy [19-22]. Yeshchenko et al. [23] in another experimental investigation, examined the melting point of AgNSPs with diameter 8-30 nm and obtained the T_m in the span of 383-640 K. They reported that the melting process firstly started with melting the outer silver atomic layer which is called surface premelting or surface melting (T_{sm}) and then the nanospheres completely was melted by raising the temperature; also, they revealed that the $T_m > T_{sm}$. However, the mechanism of this process was not obviously complete. Some theoretical models such as Shi's model [24], Hanszen's model [25], and liquid drop model [26] only are able to predicate T_m; however, cherneyshev's model can only forecast the T_{sm} [27]. Therefore, an alternative approach is needed to calculate both melt points and elucidate the melting process. To trace the melting mechanism from the surface premelting stage to complete melting, computer experiments such as molecular dynamics (MD) simulations are a powerful and valuable technique and used by many researchers to probe the thermal features [28-32], mechanical and vibration characteristics [33-39], interfacial interactions [40-42], and ionic diffusion [43-45]. Alarifi et al. [29] probed the melting process of AgNSPs with a diameter of 4-20 nm with MD simulation. They observed that the nanosphere was divided into the silver core with solid-phase and quasi-liquid layer shell by starting surface premelting. Then, by increasing temperature, the liquid shell thickness raise and the diameter of the solid core decrease. This process continues up to complete melting. Cui et al. [31] by MD simulation demonstrated the silver nanosphere with 3 nm diameter has 815 K melting temperature. The current study's research emphasizes several significant aspects within the academic field, particularly in relation to nanoparticles. These include the understanding of distinct melting mechanisms, surface premelting and complete melting points, thermal stability for antibacterial applications, and the intensive property of specific heat capacity at a constant volume. These findings greatly contribute to the existing knowledge base and offer valuable insights for the efficient design and utilization of nanoparticles in medical and antibacterial settings. Furthermore, these findings have implications for optimizing performance and stability at different temperatures. Accordingly, in the present study, the melting process, the T_{sm}, the T_m, and C_v of AgNSPs and AgNCs have been probed via using MD simulation in similar conditions. It is worth mentioning that this research is one of the first investigations that reported the thermal properties of AgNCs. This paper is structured as follows: Section 2 comprehensively details the methodology of MD simulation. Subsequently, Section 3 presents the results and discussions related to data verification, the melting mechanism of nanospheres and nanocubes, the comparison of their melting temperatures, the calculations of specific heat capacity, and their implications. In Section 4, a summary and conclusion of the findings are provided, emphasizing the significance of nanoparticle morphology in high-temperature applications.

2. Simulation and method

2.1. Nanostructure modeling

In computer experiments, molding of nanostructure due to their free surfaces is different from bulk structures. The free boundary conditions or periodic boundary conditions (PBCs) with enough vacuum distance from material surfaces can be used to consider these free surfaces. PBCs with creating the image of atoms in the up and down of simulation box walls lead to bulk behavior. However, by creating enough vacuum distance between material surface and simulation box walls, PBCs cannot affect structures and free surfaces can be made. In this research, to simulate silver bulk structure and nanoparticles, the PBCs have been applied in all directions, and the FCC lattice with a 4.09 Å lattice constant was utilized [46, 47]. In bulk structure, boundary conditions successfully created bulk manner. While, in nanoparticle structures, by locating the AgNSPs and AgNCs in the center of the simulation box and creating enough vacuum distance from simulation box walls, the free surfaces establish successfully. The details of the structures and simulation box are indicated in Table 1 and Fig. 1. To consider nanoparticles appropriate to their experimental morphologies, the AgNSPs and AgNCs have been fabricated under {111} and {100} facets, respectively [2, 13, 48,

49]. In addition, to explore the size of nanoparticle's effects on thermal attributes under similar situations, the AgNSPs and AgNCs have been considered with the commensurate number of atoms in various sizes (Table 1).

Table 1: The number of supercells (S), number of atoms (N), diameter (D), length of the cube (L), and facets directions (F.D) of bulk and nanospheres and nanocubes that used in the current research.

(a) Bulk

Sample	**S**	**N**
$Bulk_{10\times10\times10}$	10 × 10 × 10	4000

(b) Silver nanospheres (AgNSPs)

Sample	**D (nm)**	**N**	**F.D**
$AgNSP_{3.27nm}$	3.27	1061	{111}
$AgNSP_{4.09nm}$	4.09	2123	{111}
$AgNSP_{4.90nm}$	4.90	3589	{111}
$AgNSP_{5.73nm}$	5.73	5759	{111}

(c) Silver nanocubes (AgNCs)

Sample	**L (nm)**	**N**	**F. D**
$AgNC_{2.86nm}$	2.86	1372	{100}
$AgNC_{3.27nm}$	3.27	2048	{100}
$AgNC_{4.09nm}$	4.09	4000	{100}
$AgNC_{4.49nm}$	4.49	5324	{100}

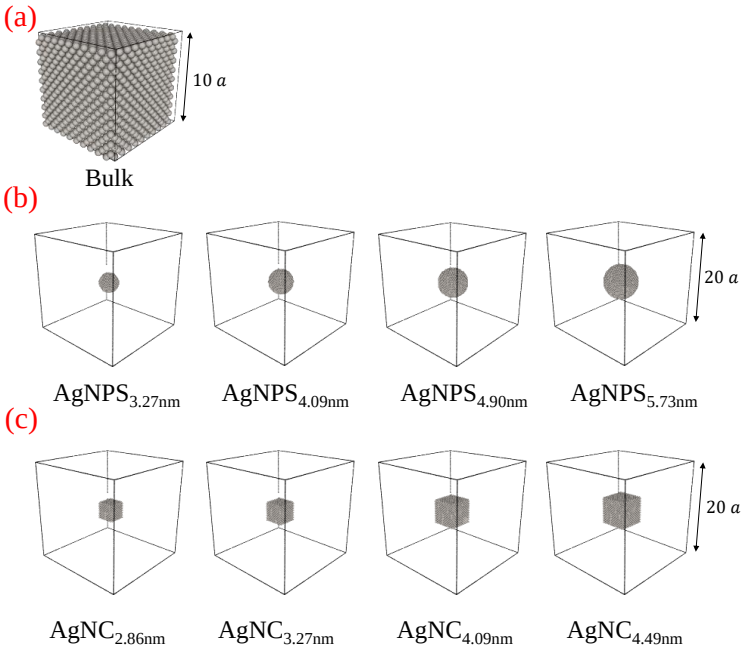

Fig 1: The initial structures and simulation box lengths of (a) silver bulk, (b) AgNSPs, and (c) AgNCs are considered in this research. The silver atoms have been demonstrated by gray color. The a is lattice constant equal to 4.09 Å.

2.2. Interaction potential

The interaction between silver atoms has been modeled by the embedded-atom method (EAM) potential [47]. The equation below illustrates the relationship of the EAM potential.

$$U_{EAM}(F,\rho,\varphi,r) = F_\alpha\left(\sum_{i\neq j}\rho_\beta(\vec{r}_{ij})\right)+\frac{1}{2}\sum_{i\neq j}\varphi_{\alpha\beta}(\vec{r}_{ij}) \quad (1)$$

Here, U_{EAM} is EAM potential function, ρ depicts the atomic electron density, F_α points to the energy to embed atom α into the background ρ and will be taken from Hartree-Pock calculations, $\vec{r}_{ij}$ signifies the distance between atoms i and j, φ represent the core-core pair repulsion potential interaction, i and j are the atom counter. α and β show the element type which for silver is Ag. The embedding energy and the core-core pair repulsion interaction are related to the first and second terms of Eq. (1), respectively. The EAM potential as a semi-empirical method was firstly proposed by Daw and Baskes [50, 51] based on density functional ideas and can model the physical features of silver bulk and nanostructures successfully [29, 47, 52]. EAM potential with suitable simulation speed, low simulation cost, and an appropriate agreement with experiments is powerful potential for atomistic simulation of silver as a metallic system.

2.3. MD simulation setups

In the current investigation, to explore thermal characteristics of silver bulk and nanoparticles, all MD simulations performed by large-scale atomic/molecular massively parallel simulator (LAMMPS) package [53] and the structures visualized by open visualization tool (OVITO) [54]. All structures have been simulated with 1 femtosecond timestep and Nose`-Hoover thermostat (NVT). Also, the equation motions are solved by using the velocity-Verlet algorithm [55]. For simulations, first of all, the initial configurations were made based on section 2.1, then, at a room temperature (300 K), the initial velocities of atoms created via Maxwell-Boltzmann distribution [56]. In the following, the structures have simulated in the two stages: equilibrium and heating stages. In the equilibrium stage, the structures equilibrated under NVT ensemble at 300 K for 1 nanosecond. This time is long enough to achieve the thermodynamic equilibrium. In the heating stage, the temperature raised under NVT ensemble from 300 to 1500 K with a heating rate of 1.2 K/ps during 1 ns. The heating rate was chosen with respect to simulation accuracy and efficiency. The large and small heating rates lead to thermal shock and longtime simulation, respectively. The 1.2 K/ps for heating rate lead to converging bulk melt point with experimental data, elimination thermal shock, suitable simulation accuracy, and good performance [57].

3. Results and discussion

3.1. Data verification

Initially, the melting point of silver bulk probed to assess the simulation results. So, during the heating stage, the potential energy and temperature are calculated. Then the potential energy is divided into the number of atoms to calculate the potential energy per atom (PPA). By drawing PPA against temperature, each sharp jumping in this curve indicates the phase transition, and melting point can be measured. Fig. 2.a illustrates the melting process of silver bulk. It is clear from this curve that the PPA raised linearly by increasing temperature, and in the 1200 K, the sharp jumping observed in PPA means silver is going to be melted. Comparing the value of the bulk melting point from the present study and 1234 K from the experiment [19] display satisfactory agreement and validity of results. The difference between the experimental and calculated values can back to the limitation of calculation melting point of bulk materials by simulation methods. In the bulk simulation, there is no surface, and all atoms are heated by increasing temperature. In contrast, in the actual experiment, the melting process always began from the surface, and the atoms located on the surface heated firstly. This restriction causes the difference between calculated bulk melting points from experimental and computational methods. In addition to the melting point, the specific heat capacity at constant pressure (C_p) is obtained by calculating enthalpy splitting it to the mass of all atoms, and drawing it against temperature. The slope of this curve indicates the C_p is dependent on temperature and pressure [58]. To compare the C_p with experimental data

at room temperature, C_p has been obtained by calculating the slope of the enthalpy curve in the range of 300-320 K. The obtained C_p is 240 $\frac{J}{Kg.K}$ that is in good agreement with experimental 236 $\frac{J}{Kg.K}$ [59].

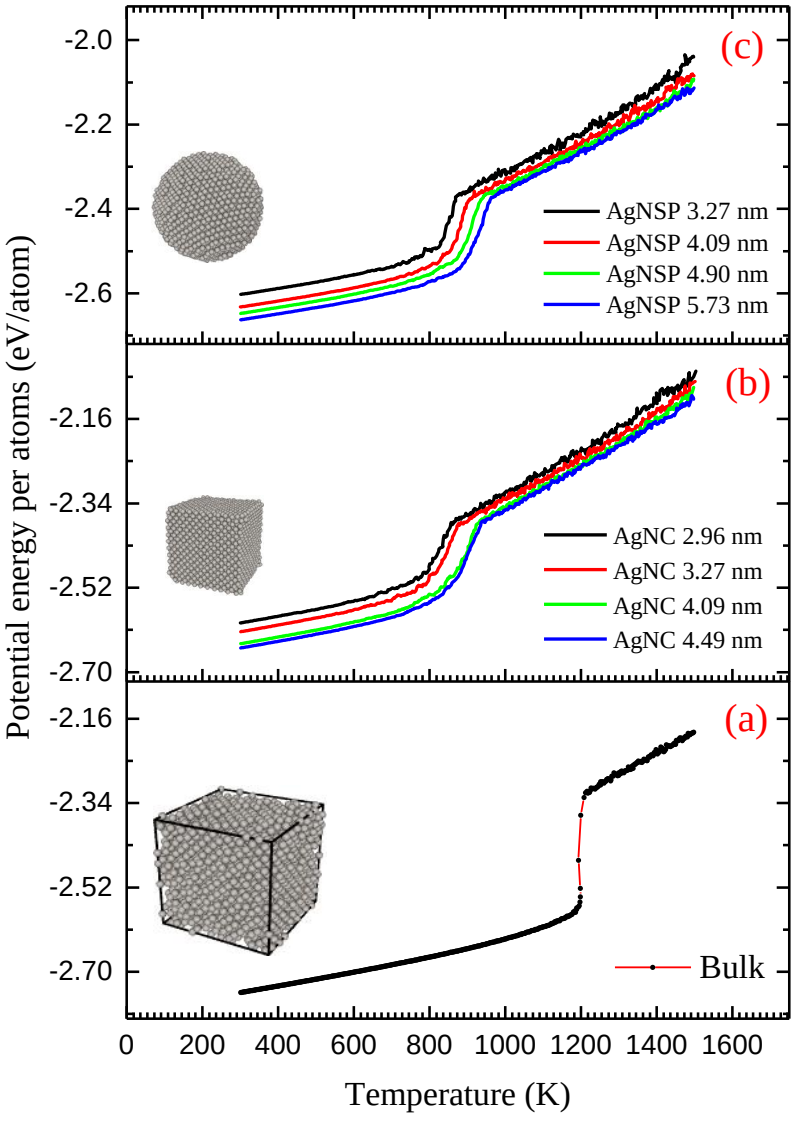

Fig 1: The potential energy per atoms (PPA) against the corresponding temperature during heating stage (a) silver bulk, (b) AgNCs, and (c) AgNSPs

3.2. Nanoparticles melting mechanism

3.2.1. Nanospheres melting mechanism

To elucidate the nanoparticles phase transition mechanism, Fig. 3 indicates the melting curves, the corresponding atomic arrangements, and corresponding radial distribution functions (RDF) curve at different temperatures for $AgNSP_{5.73nm}$ and $AgNC_{4.49nm}$. The atomic arrangement indicates cutting a cross-section in the [001] direction at the center of nanoparticles with 1 nm thickness. This thickness is long enough to clarify the crystallographic planes of the nanoparticles.

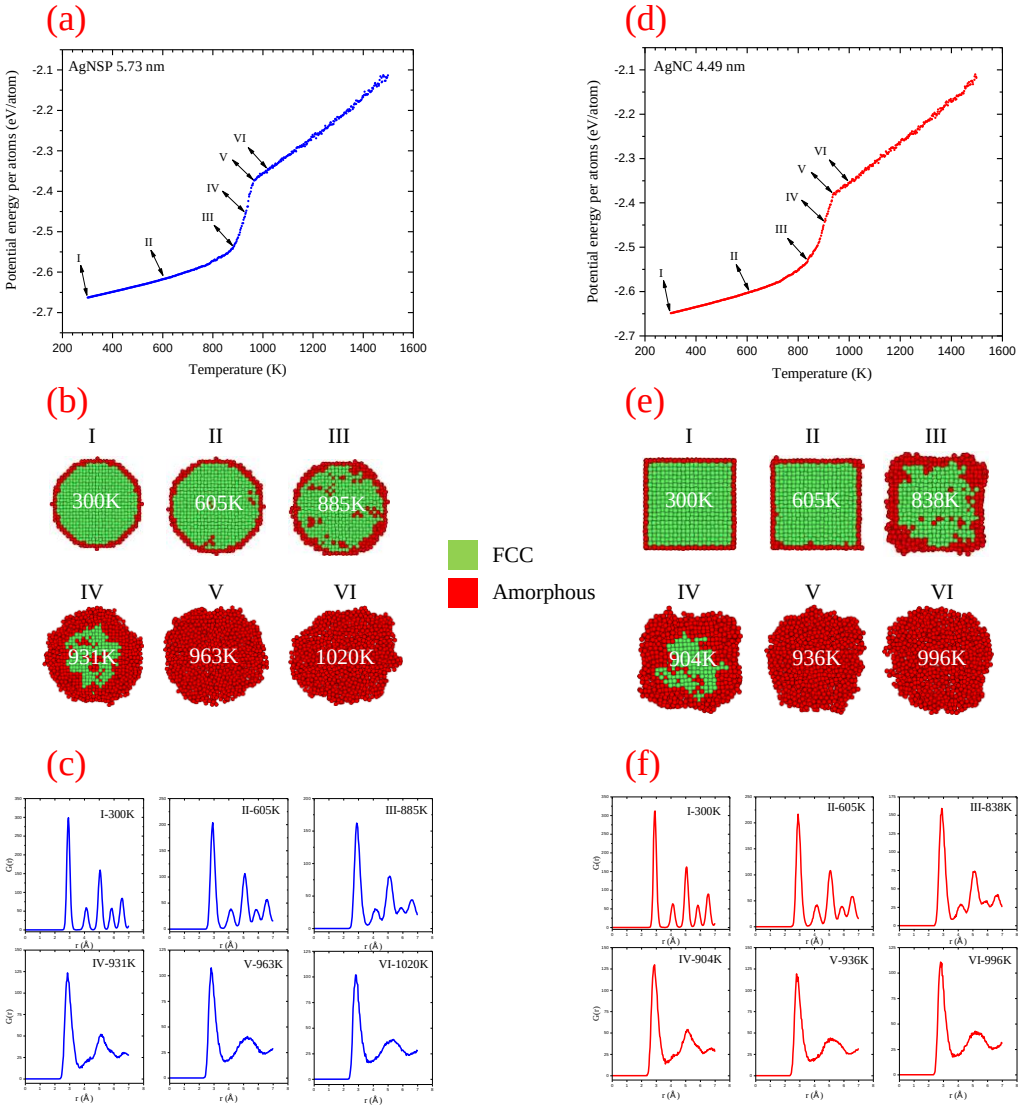

Fig 2: The melting curve, the corresponding atomic arrangements, and corresponding radial distribution function (RDF) curve of $AgNSP_{5.73nm}$ (a, b, c), and $AgNC_{4.49nm}$ (d, e, f) at different temperatures.

Fig. 3.a demonstrates the melting curve of $AgNSP_{5.73nm}$. In this figure, six temperatures at different stages have been examined. Stage I is corresponding to 300 K temperature. Obviously, by enhancing temperature, the PPA raised linearly and reach stage II with 605 K. Between the I and II stages, the slope of the melting curve is almost the same; however, in stage III with 885 K, the slope of the curve changes (this temperature can be the T_{sm}, but to be sure, the corresponding atomic arrangements and RDF must be analyzed). This slope from stage III to V continues, and in stage

V with 963 K, the slope changes again. In stage V, it can be express that the nanosphere is melted completely. Between V and VI stages, the curve slope unchanged, and after stage VI continue to be the same. To analyze these six stages accurately, the atomic arrangement of $AgNSP_{5.73nm}$ corresponds to these stages demonstrated in Fig. 3.b. It is clear from this figure that in the I and II stages the outer ultra-thin shell is amorphous and the core is in FCC lattice. In stage III, the thickness of the amorphous shell is raised, which shows the surface premelting began from this stage. In stage IV the amorphous shell significantly has been raised, and the $AgNSP_{5.73nm}$ split into a solid core with FCC lattice and liquid amorphous shell. By tracing stages III to IV, it can be concluded that the nanosphere melted gradually in the direction of the nanosphere radius. In stage V all of the cross-sectional has amorphous phase, and the structure completely melted. This point indicates the T_m. Stage VI shows that after stage V, $AgNSP_{5.73nm}$ has the liquid phase with amorphous morphology. RDF is a valuable and reliable curve to assess the solid, liquid, or gas phases. The RDF curve shows how and probability of distribution of atoms as a function of distance from a reference atom, and can confirm the atomic arrangement data with high accuracy. If the RDF diagram includes several sharp peaks, the phase of a substance is solid, and the first peak shows the distance from the first neighbor in the crystal lattice, and so on. If RDF indicates one approximately sharp peak and the second average peak, the material phase is liquid. If RDF illustrates one small peak, it reveals the gas phase. Therefore, the RDF, which can be the appropriate equivalent of X-ray spectra in numerical simulation, has been utilized as an effective indicator for distinguishing among different phases including solid, liquid, or gas [52]. Fig. 3.c demonstrates the RDF curve of the $AgNSP_{5.73nm}$ corresponding to the six stages mentioned earlier. In the I and II stages, the RDF curve indicates several regular sharp peaks, which describe that the phase of $AgNSP_{5.73nm}$ is completely solid. In stage III, the high peaks decrease, which describes the surface premelting started from this stage. In stage IV, two peaks obtained, but around the second peak, two areas were observed. The curve conduct in this stage shows the solid and liquid phases exist together, and the dominant volume of $AgNSP_{5.73nm}$ is the liquid phase. In stage V, only one approximately sharp peak can be seen, and the curve reveals the liquid phase of the nanosphere. The temperature of this stage is T_m. In stage VI, the manner of stage V is repeated and shows that after the complete melting, the phase of the nanosphere is entirely liquid. In summary, based on Fig. 3(a-c), it can conclude that: from stages I to III the nanoparticles heated and the kinetic energy of atoms increases, in stage III the surface premelting began and the temperature of this stage is T_{sm}, in the range of stages III to V the material completely be melted and the temperature of stage V is the T_m, and after stage V the phase is liquid. For other AgNSPs, similar conduct at different temperatures is observed.

3.2.2. Nanocubes melting mechanism

Fig. 3(d-f) illustrate the melting curve, the corresponding atomic arrangements, and corresponding RDF curve at different temperatures of $AgNC_{4.49nm}$, respectively. The analysis of these curves is similar to $AgNSP_{5.73nm}$; however, $AgNC_{4.49nm}$ has lower T_{sm} and T_m than $AgNSP_{5.73nm}$. Also, in $AgNC_{4.49nm}$, the surface premelting commences from the corners of the cube. Simultaneously, with surface premelting, the amorphous shell formed and then enhanced toward the nanocube center by increasing temperature. For other AgNCs, the same behavior at various temperatures was observed.

3.2.3. Comparison of T_{sm} and T_m of nanospheres and nanocubes

Fig. 2(b-c) illustrate the melting process of AgNCs and AgNSPs, respectively. Based on these figures, unlike bulk behavior, the phase transition of nanoparticles from solid to liquid performs gradually. This manner is detected because of the surface premelting of nanoparticles. Like $AgNSP_{5.73nm}$ and $AgNC_{4.49nm}$, the T_{sm} and T_m were obtained for other nanospheres and nanocubes and summarized in Table 2. This table indicates that between nanospheres and nanocubes with a similar number of atoms, nanocubes have lower T_{sm} and T_m than nanospheres due to the high surface free energy of planes and active planes in the [100] direction [60]. The high surface free energy cause that with enhancing temperature, the amplitude of atomic vibration increasing more than the lattice constant, which makes nanocubes melted earlier. The differences in melting points and thermal behavior of silver nanospheres and nanocubes can significantly affect their effectiveness in real-world scenarios for antibacterial applications and life in extreme environments [61, 62]. The research findings indicate that the geometry of nanoparticles plays a crucial role in determining their thermal stability. Nanocubes have lower T_{sm} and T_m compared to nanospheres. Additionally, the melting process of nanocubes starts from their corners and progresses towards the center of the cube, whereas nanospheres melt from the surface towards the core in the radial direction. This distinction in melting behavior implies that nanocubes are more susceptible to melting and losing their structural integrity at lower temperatures compared to

nanospheres. As a result, in applications where nanoparticles are exposed to elevated temperatures, nanospheres might be more suitable due to their higher thermal stability.

Table 2: The comparison of a number of atoms (N), surface premelting, T_{sm}(K), complete melting point, T_m(K), and specific heat capacity at a constant volume, $C_v(\frac{J}{Kg.K})$, of silver nanospheres and nanocubes in the current investigation.

Nanospheres

$AgNSP_{3.27nm}$				$AgNSP_{4.09nm}$				$AgNSP_{4.49nm}$				$AgNSP_{5.73nm}$			
N	T_{sm}	T_m	C_v	N	T_{sm}	T_m	C_v	N	T_{sm}	T_m	C_v	N	T_{sm}	T_m	C_v
1061	826	871	240	2123	850	903	242	3589	865	936	241	5759	885	963	242

Nanocubes

$AgNC_{2.86nm}$				$AgNC_{3.27nm}$				$AgNC_{4.09nm}$				$AgNC_{4.49nm}$			
N	T_{sm}	T_m	C_v	N	T_{sm}	T_m	C_v	N	T_{sm}	T_m	C_v	N	T_{sm}	T_m	C_v
1372	783	864	240	2048	802	887	239	4000	827	927	240	5324	838	936	240

3.2.4. Mean square displacement behavior of nanoparticles under a melting mechanism

The displacement of atoms can be calculated over time with mean square displacement (MSD) [29]. In solid, liquid, and gas phases, the MSD of atoms is different, and the sequence of MSD in these phases are in the order of gas > liquid > solid. Therefore, during the heating stage, if MSD plots against temperature, then each shift in MSD reveals the phase transition. Fig. 4 demonstrates the MSD curve of AgNSPs and AgNCs against temperature during the melting process. In all these curves, it is apparent that the slope of MSD is the same up to T_{sm}. Then from T_{sm} to T_m the slope of the curve alters (this limited region is shown with red color on MSD curves), and after T_m, the slope remains the same. Changing MSD slope in the range of T_{sm} to T_m indicates the melting process occurs between these temperatures.

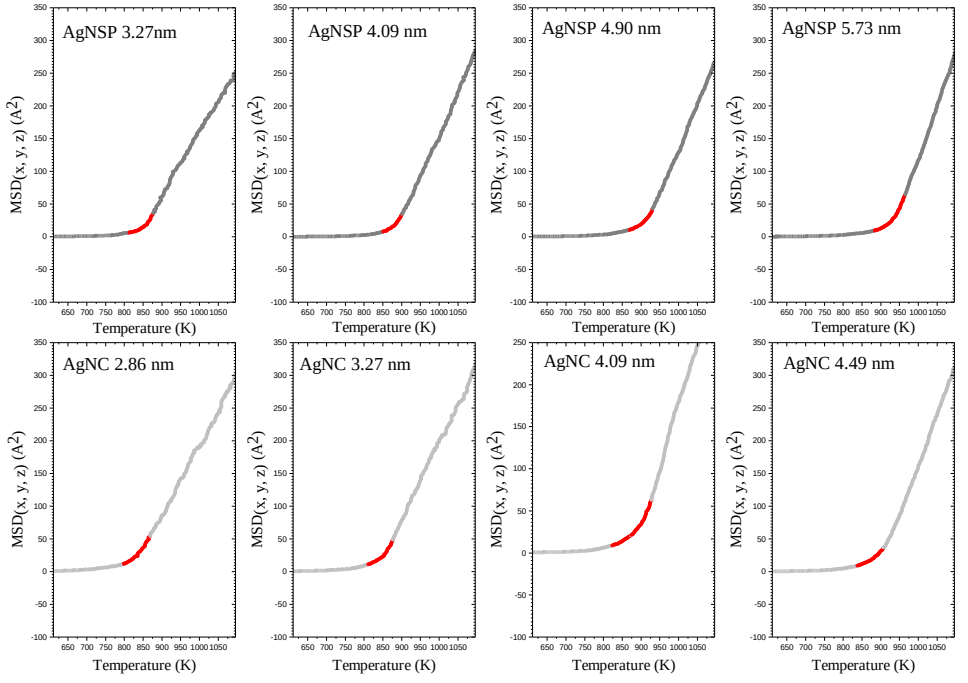

Fig 3: The MSD curves of silver nanospheres and nanocubes against temperature during the heating stage. The red color shows the limited region of the melting process.

3.3. The specific heat capacity at a constant volume of nanoparticles

The specific heat capacity at a constant volume, $C_v(T)$, by a unit of $\frac{J}{Kg.K}$ is defined as the amount of energy (heat) that transfers into or out of the unit of substance to increase or decrease the temperature at a constant volume. This parameter can be obtained by using the below thermodynamic relation [58, 59]:

$$C_V(T) = (\frac{\partial U}{\partial T})_V \quad (2)$$

Which U is the total energy split to the mass of atoms by unit of $\frac{J}{Kg}$, and T is temperature by the unit of K. To use this relation to calculate $C_v(T)$, during the heating stage, the total energy of nanoparticles must be calculated and split to the mass of silver atoms, and then this value should be plotted against temperature. The slope of this curve shows the $C_v(T)$ and depends on the temperature at constant volume. In almost all medical antibacterial applications, the silver nanoparticles are utilized at room temperature because the antimicrobial activity decreases at high temperatures [63]. Thus, to obtain $C_v(T)$ related to room temperature, this parameter was measured in the range of 300-320 K. Fig. 5 illustrates the curve of $AgNSP_{5.73nm}$ total energy versus temperature and fitting region for calculation $C_v(T)$. For other nanospheres and nanocubes, the $C_v(T)$ was calculated similarly and summarized in Table 2. Comparison of $C_v(T)$ values reveal that this parameter is independent of the shape and size of nanoparticles. Also, this parameter is close to the value of C_p in silver bulk. These results disclose that the $C_v(T)$ and C_p have slight differences together [59]. Moreover, by decreasing the silver dimension from bulk to nanoparticles, the C_v remains the same, which shows that the $C_v(T)$ is an intensive property.

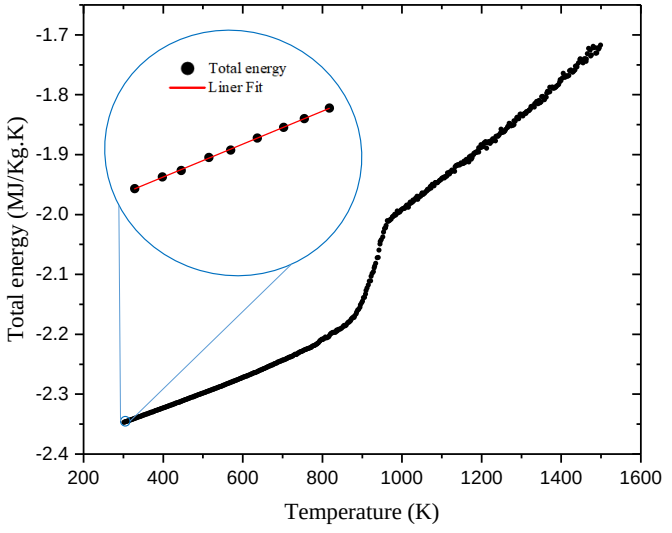

Fig 4: The curve of $AgNSP_{5.73nm}$ total energy against temperature. The region from 300 to 320 K has been demonstrated in the curve. The melting process also can be observed from the total energy curve like the melting curve in **Fig 2**.

4. Summary and conclusion

In this research, the melting process and the specific heat capacity at a constant volume of silver nanospheres and nanocubes, which have antibacterial applications, have been investigated via molecular dynamics simulation technique. The results indicate that the melting process begins from the surface of nanospheres toward the core in the radius direction; however, nanocubes melt from the corners toward the center of the cube. Moreover, nanocubes owing to their high surface free energy of planes and active planes in the [100] direction, have lower surface premelting

and complete melting points than nanospheres. These represents that nanocubes have lower thermal stability in comparison with nanospheres. So, the nanospheres are more stable at high temperature for antibacterial applications. The specific heat capacity at a constant volume of nanospheres and nanoparticles are almost identical and are close to the bulk value, which shows this parameter as an intensive property independent of the size and shape of nanoparticles.

References

[1] L. Mulfinger, S. D. Solomon, M. Bahadory, A. V. Jeyarajasingam, S. A. Rutkowsky, C. Boritz, Synthesis and Study of Silver Nanoparticles, *Journal of Chemical Education*, Vol. 84, No. 2, pp. 322, 2007/02/01, 2007.

[2] D. Yu, V. W.-W. Yam, Controlled Synthesis of Monodisperse Silver Nanocubes in Water, *Journal of the American Chemical Society*, Vol. 126, No. 41, pp. 13200-13201, 2004/10/01, 2004.

[3] H.-W. Jang, B.-Y. Hwang, K.-W. Lee, Y.-M. Kim, J.-Y. Kim, Controlling the size of silver nanowires produced by a tetrabutylammonium dichlorobromide salt-based polyol process: Kinetics of silver crystal growth, *AIP Advances*, Vol. 8, No. 2, pp. 025303, 2018.

[4] A. Ghafouri Pourkermani, B. Azizi, H. Nejat Pishkenari, Vibrational analysis of Ag, Cu and Ni nanobeams using a hybrid continuum-atomistic model, *International Journal of Mechanical Sciences*, Vol. 165, pp. 105208, 2020/01/01/, 2020.

[5] Z. Rakocevic, R. Petrovic, S. Strbac, Surface roughness of ultra-thin silver films sputter depositedon a glass, *Journal of Microscopy*, Vol. 232, No. 3, pp. 595-600, 2008/12/01, 2008.

[6] J.-M. Liu, X.-P. Yan, Competitive aptamer bioassay for selective detection of adenosine triphosphate based on metal-paired molecular conformational switch and fluorescent gold nanoclusters, *Biosensors and Bioelectronics*, Vol. 36, No. 1, pp. 135-141, 2012/06/01/, 2012.

[7] S. Chernousova, M. Epple, Silver as Antibacterial Agent: Ion, Nanoparticle, and Metal, *Angewandte Chemie International Edition*, Vol. 52, No. 6, pp. 1636-1653, 2013/02/04, 2013.

[8] M. Chen, I. Y. Phang, M. R. Lee, J. K. W. Yang, X. Y. Ling, Layer-By-Layer Assembly of Ag Nanowires into 3D Woodpile-like Structures to Achieve High Density "Hot Spots" for Surface-Enhanced Raman Scattering, *Langmuir*, Vol. 29, No. 23, pp. 7061-7069, 2013/06/11, 2013.

[9] Y. Tang, W. He, S. Wang, Z. Tao, L. Cheng, One step synthesis of silver nanowires used in preparation of conductive silver paste, *Journal of Materials Science: Materials in Electronics*, Vol. 25, No. 7, pp. 2929-2933, 2014/07/01, 2014.

[10] I. X. Yin, J. Zhang, I. S. Zhao, M. L. Mei, Q. Li, C. H. Chu, The Antibacterial Mechanism of Silver Nanoparticles and Its Application in Dentistry, *International Journal of Nanomedicine*, Vol. 15, pp. 2555-2562, 2020/12/01, 2020.

[11] P. Prosposito, L. Burratti, I. Venditti, Silver Nanoparticles as Colorimetric Sensors for Water Pollutants, *Chemosensors*, 8, 2020.

[12] J. Kim, S. H. Lee, H. Kim, S. H. Kim, C. E. Park, 3D Hollow Framework Silver Nanowire Electrodes for High-Performance Bottom-Contact Organic Transistors, *ACS Applied Materials & Interfaces*, Vol. 7, No. 26, pp. 14272-14278, 2015/07/08, 2015.

[13] X. Hong, J. Wen, X. Xiong, Y. Hu, Shape effect on the antibacterial activity of silver nanoparticles synthesized via a microwave-assisted method, *Environmental Science and Pollution Research*, Vol. 23, No. 5, pp. 4489-4497, 2016/03/01, 2016.

[14] M. Halder, A. K. Meikap, Influence on loading terbium manganate on optical, thermal and electrical properties of polyvinyl alcohol nanocomposite films, *Journal of Materials Science: Materials in Electronics*, Vol. 30, No. 5, pp. 4792-4806, 2019/03/01, 2019.

[15] S. Singh, A. Bharti, V. K. Meena, Structural, thermal, zeta potential and electrical properties of disaccharide reduced silver nanoparticles, *Journal of Materials Science: Materials in Electronics*, Vol. 25, No. 9, pp. 3747-3752, 2014/09/01, 2014.

[16] B. N. Khlebtsov, V. A. Khanadeev, I. L. Maksimova, G. S. Terentyuk, N. G. Khlebtsov, Silver nanocubes and gold nanocages: Fabrication and optical and photothermal properties, *Nanotechnologies in Russia*, Vol. 5, No. 7, pp. 454-468, 2010/08/01, 2010.

[17] M. Asoro, J. Damiano, P. J. Ferreira, Size Effects on the Melting Temperature of Silver Nanoparticles: In-Situ TEM Observations, *Microscopy and Microanalysis*, Vol. 15, No. S2, pp. 706-707, 2009.

[18] M. A. Asoro, D. Kovar, J. Damiano, P. J. Ferreira, Scale Effects on the Melting Behavior of Silver Nanoparticles, *Microscopy and Microanalysis*, Vol. 16, No. S2, pp. 1802-1803, 2010.
[19] A. D. Kirshenbaum, J. A. Cahill, A. V. Grosse, The density of liquid silver from its melting point to its normal boiling point 2450°K, *Journal of Inorganic and Nuclear Chemistry*, Vol. 24, No. 3, pp. 333-336, 1962/03/01/, 1962.
[20] G. L. Allen, R. A. Bayles, W. W. Gile, W. A. Jesser, Small particle melting of pure metals, *Thin Solid Films*, Vol. 144, No. 2, pp. 297-308, 1986/11/15/, 1986.
[21] Q. S. Mei, K. Lu, Melting and superheating of crystalline solids: From bulk to nanocrystals, *Progress in Materials Science*, Vol. 52, No. 8, pp. 1175-1262, 2007/11/01/, 2007.
[22] K. Kang, S. Qin, C. Wang, Size-dependent melting: Numerical calculations of the phonon spectrum, *Physica E: Low-dimensional Systems and Nanostructures*, Vol. 41, No. 5, pp. 817-821, 2009/03/01/, 2009.
[23] O. A. Yeshchenko, I. M. Dmitruk, A. A. Alexeenko, A. V. Kotko, Surface plasmon as a probe for melting of silver nanoparticles, *Nanotechnology*, Vol. 21, No. 4, pp. 045203, 2009/12/10, 2010.
[24] F. G. Shi, Size dependent thermal vibrations and melting in nanocrystals, *Journal of Materials Research*, Vol. 9, No. 5, pp. 1307-1313, 1994/05/01, 1994.
[25] K. J. Hanszen, Theoretische Untersuchungen über den Schmelzpunkt kleiner Kügelchen, *Zeitschrift für Physik*, Vol. 157, No. 5, pp. 523-553, 1960/10/01, 1960.
[26] K. K. Nanda, S. N. Sahu, S. N. Behera, Liquid-drop model for the size-dependent melting of low-dimensional systems, *Physical Review A*, Vol. 66, No. 1, pp. 013208, 07/29/, 2002.
[27] A. P. Chernyshev, Effect of nanoparticle size on the onset temperature of surface melting, *Materials Letters*, Vol. 63, No. 17, pp. 1525-1527, 2009/07/15/, 2009.
[28] S. Alavi, 2020, *Molecular simulations: fundamentals and practice*, John Wiley & Sons,
[29] H. A. Alarifi, M. Atiş, C. Özdoğan, A. Hu, M. Yavuz, Y. Zhou, Determination of Complete Melting and Surface Premelting Points of Silver Nanoparticles by Molecular Dynamics Simulation, *The Journal of Physical Chemistry C*, Vol. 117, No. 23, pp. 12289-12298, 2013/06/13, 2013.
[30] Z. Qiao, H. Feng, J. Zhou, Molecular dynamics simulations on the melting of gold nanoparticles, *Phase Transitions*, Vol. 87, No. 1, pp. 59-70, 2014/01/02, 2014.
[31] J. Cui, L. Yang, Y. Wang, Molecular Dynamics Simulation Study of the Melting of Silver Nanoparticles, *Integrated Ferroelectrics*, Vol. 145, No. 1, pp. 1-9, 2013/01/01, 2013.
[32] Z. Ahadi, M. Shadman Lakmehsari, S. Kumar Singh, J. Davoodi, Stability and thermal behavior of molybdenum disulfide nanotubes: Nonequilibrium molecular dynamics simulation using REBO potential, *Journal of Applied Physics*, Vol. 122, No. 22, pp. 224303, 2017.
[33] B. Azizi, S. Rezaee, M. J. Hadianfard, K. H. Dehnou, A comprehensive study on the mechanical properties and failure mechanisms of graphyne nanotubes (GNTs) in different phases, *Computational Materials Science*, Vol. 182, pp. 109794, 2020/09/01/, 2020.
[34] M. Kohestanian, Z. Sohbatzadeh, S. Rezaee, Mechanical properties of continuous fiber composites of cubic silicon carbide (3C-SiC) / different types of carbon nanotubes (SWCNTs, RSWCNTs, and MWCNTs): A molecular dynamics simulation, *Materials Today Communications*, Vol. 23, pp. 100922, 2020/06/01/, 2020.
[35] R. Momen, R. Rezaee, B. Azizi, S. Rezaee, H. Hou, X. Ji, Evaluation of mechanical properties of multilayer graphyne-based structures as anode materials for lithium-ions batteries, *Eur. Phys. J. Plus*, Vol. 137, No. 3, //, 2022.
[36] B. Azizi, M. Shariati, S. S. M. N. Souq, M. Hosseini, Bending and stretching behavior of graphene structures using continuum models calibrated with modal analysis, *Applied Mathematical Modelling*, Vol. 114, pp. 466-487, 2023/02/01/, 2023.
[37] M. Shariati, S. S. M. N. Souq, B. Azizi, Surface- and nonlocality-dependent vibrational behavior of graphene using atomistic-modal analysis, *International Journal of Mechanical Sciences*, Vol. 228, pp. 107471, 2022/08/15/, 2022.
[38] M. Shariati, B. Azizi, M. Hosseini, M. Shishesaz, On the calibration of size parameters related to non-classical continuum theories using molecular dynamics simulations, *International Journal of Engineering Science*, Vol. 168, pp. 103544, 2021/11/01/, 2021.
[39] B. Azizi, M. Hosseini, M. Shariati, On the hybrid atomistic-continuum model for vibrational analysis of α-, β-, and γ-graphyne circular nano-plates, *Waves in Random and Complex Media*, pp. 1-36, 2022.
[40] N. Ertekin, S. Rezaee, B. Azizi, Mechanical properties and role of 2D alkynyl carbon monolayers in the progress of lithium-air batteries, *Journal of Energy Storage*, Vol. 72, pp. 108558, 2023/11/25/, 2023.

[41] M. Ghoohestani, S. Rezaee, E. Kadivar, M. A. Esmaeilbeig, Reactive-dynamic characteristics of a nanobubble collapse near a solid boundary using molecular dynamic simulation, *Physics of Fluids*, Vol. 35, No. 2, pp. 022003, 2023.

[42] M. Ghoohestani, S. Rezaee, E. Kadivar, O. el Moctar, Thermodynamic effects on nanobubble's collapse-induced erosion using molecular dynamic simulation, *Physics of Fluids*, Vol. 35, No. 7, pp. 073319, 2023.

[43] H. Araghi, S. Rezaee, Z. Zabihi, Ionic conductivity of oxygen in BaTiO3, Ba0.9A0.1TiO3-δ (A: Li+, Na+, Ca2+), and BaTi0.9B0.1O3-δ (B: V3+, Cr3+, Si4+) crystals with cubic perovskite structure as cathode in fuel cell: A molecular dynamics study, *Journal of Solid State Chemistry*, Vol. 258, pp. 640-646, 2018/02/01/, 2018.

[44] N. Ertekin, S. Rezaee, Lithium-Doped Barium Titanate as Advanced Cells of ReRAMs Technology, *Journal of Electronic Materials*, Vol. 52, No. 2, pp. 1575-1589, 2023/02/01, 2023.

[45] N. Ertekin, S. Rezaee, Effect of anion and cation vacancies pairs in conduct of the Ba1−3xTiO31−x and BaTi(1−3x2)O3(1−x) (x = 0.0033) as a memristor, *Materials Today Communications*, Vol. 31, pp. 103333, 2022/06/01/, 2022.

[46] N. Ashcroft, N. Mermin, Solid State Physics, Holt, Rinehart and Winston, *New York*, Vol. 2005, pp. 403, 1976.

[47] S. M. Foiles, M. I. Baskes, M. S. Daw, Embedded-atom-method functions for the fcc metals Cu, Ag, Au, Ni, Pd, Pt, and their alloys, *Physical Review B*, Vol. 33, No. 12, pp. 7983-7991, 06/15/, 1986.

[48] M. M. Blazhynska, A. Kyrychenko, O. N. Kalugin, Molecular dynamics simulation of the size-dependent morphological stability of cubic shape silver nanoparticles, *Molecular Simulation*, Vol. 44, No. 12, pp. 981-991, 2018/08/13, 2018.

[49] Y. Dong, Y. Xie, L. Hu, C. Xu, W. Guo, G. Pan, Q. Wang, F. Qian, J. Sun, Graphene-assisted preparation of large-scale single-crystal Ag(111) nanoparticle arrays for surface-enhanced Raman scattering, *Nanotechnology*, Vol. 32, No. 2, pp. 025301, 2020/10/12, 2021.

[50] M. S. Daw, M. I. Baskes, Semiempirical, Quantum Mechanical Calculation of Hydrogen Embrittlement in Metals, *Physical Review Letters*, Vol. 50, No. 17, pp. 1285-1288, 04/25/, 1983.

[51] M. S. Daw, M. I. Baskes, Embedded-atom method: Derivation and application to impurities, surfaces, and other defects in metals, *Physical Review B*, Vol. 29, No. 12, pp. 6443-6453, 06/15/, 1984.

[52] V. G. Grigoryan, D. Alamanova, M. Springborg, Structure and energetics of Cu_N clusters with ($2 \leq N \leq 150$) : An embedded-atom-method study, *Physical Review B*, Vol. 73, No. 11, pp. 115415, 03/15/, 2006.

[53] S. Plimpton, Fast Parallel Algorithms for Short-Range Molecular Dynamics, *Journal of Computational Physics*, Vol. 117, No. 1, pp. 1-19, 1995/03/01/, 1995.

[54] A. Stukowski, Visualization and analysis of atomistic simulation data with OVITO–the Open Visualization Tool, *Modelling and Simulation in Materials Science and Engineering*, Vol. 18, No. 1, pp. 015012, 2009/12/15, 2010.

[55] W. C. Swope, H. C. Andersen, P. H. Berens, K. R. Wilson, A computer simulation method for the calculation of equilibrium constants for the formation of physical clusters of molecules: Application to small water clusters, *The Journal of Chemical Physics*, Vol. 76, No. 1, pp. 637-649, 1982.

[56] S. Rezaee, H. Araghi, H. Noshad, Z. Zabihi, Physical characteristics of fluorine-doped lithium oxide as advanced material for solid-electrolyte-interphase applications of lithium–air batteries, *The European Physical Journal Plus*, Vol. 137, No. 10, pp. 1194, 2022/10/29, 2022.

[57] S. Rezaee, H. Araghi, H. Noshad, Z. Zabihi, Physical characteristics of nickel thin-films and nickel thin-film foams as Li-air batteries anode and cathode current collectors, *Journal of Molecular Liquids*, Vol. 383, pp. 122171, 2023/08/01/, 2023.

[58] M. W. Zemansky, R. Dittman, Heat and thermodynamics: an intermediate textbook, *(No Title)*, 1968.

[59] D. Halliday, R. Resnick, J. Walker, 2013, *Fundamentals of physics*, John Wiley & Sons,

[60] W. Luo, W. Hu, S. Xiao, Size Effect on the Thermodynamic Properties of Silver Nanoparticles, *The Journal of Physical Chemistry C*, Vol. 112, No. 7, pp. 2359-2369, 2008/02/01, 2008.

[61] R. Amils, C. Ellis-Evans, H. Hinghofer-Szalkay, 2007, *Life in extreme environments*, Springer,

[62] F. Robb, G. Antranikian, D. Grogan, A. Driessen, 2007, *Thermophiles: biology and technology at high temperatures*, CRC Press,

[63] P. Pourali, M. Baserisalehi, S. Afsharnezhad, J. Behravan, R. Ganjali, N. Bahador, S. Arabzadeh, The effect of temperature on antibacterial activity of biosynthesized silver nanoparticles, *BioMetals*, Vol. 26, No. 1, pp. 189-196, 2013/02/01, 2013.